Crystal Structure of $Pb_2V_3O_9$: Rietveld Refinement and Electron Lone-Pair Localization. The Magnetic Susceptibility of Sr^{2+}-Substituted Phases

Olivier Mentré,* Anne Claire Dhaussy, and Francis Abraham

Laboratoire de Cristallochimie et Physicochimie du Solide URA CNRS 452 ENSCL, Université des Sciences et Technologies de Lille, BP 108, 59652 Villeneuve d'Ascq Cedex, France

Emmanuelle Suard

Institute Laue-Langevin, Rue des Martyrs, B. P. 156X, 38042 Grenoble Cedex 9, France

Hugo Steinfink

Texas Materials Institute, Department of Chemical Engineering, University of Texas at Austin, Austin, Texas 78712-1063

Received February 4, 1999. Revised Manuscript Received June 14, 1999

Powder neutron and X-ray diffraction data from $Pb_2V_3O_9$ were collected and used for structure refinement. The triclinic lattice parameters from neutron data are $a = 7.5935(1)$ Å, $b = 16.3898(3)$ Å, $c = 6.9696(1)$ Å, $\alpha = 91.41(1)°$, $\beta = 119.34(1)°$, $\gamma = 90.49(1)°$, $C\bar{1}$, and $z = 2$. The nonstandard unit cell was chosen for comparison with the monoclinic structure of $Sr_2V_3O_9$ with which it is nearly isostructural. The $6s^2$ electrons of Pb^{2+} cause the lowering of the symmetry and distort the cooperative arrangement of the vanadyl bonds existing in the V−O framework of $Sr_2V_3O_9$. One of the two crystallographically independent Pb^{2+} is in a distorted, capped, octahedral environment formed by seven oxygen atoms with Pb−O bonds ranging from 1.426(8) Å to 2.830(8) Å. The other Pb^{2+} is surrounded by nine oxygen atoms that form a distorted, tricapped, trigonal prism with Pb−O ranging from 2.421(11) to 2.920-(8). The lone-pair $6s^2$ electrons were located and are about 0.58 Å from the nucleus. Of the four crystallographically independent vanadium atoms, two are in tetrahedral coordination with a mean oxidation number +5. The other two are in octahedral coordination with oxidation number +4. The octahedra link by corner sharing into an infinite chain parallel to [101]. The tetrahedra share corners with the octahedra to form two-dimensional sheets that are then joined by the Pb ions into a three-dimensional structure. One octahedral V^{4+} cation shows displacement from its polyhedral center toward an oxygen that is corner-shared in the octahedral chain, giving rise to a short vanadyl bond, 1.67(4) Å, and a long bond of 2.18(4) Å. The main difference between the lead and strontium vanadate framework is in the displacement of the second V^{4+} ion toward an oxygen that is corner-shared with a tetrahedron. Here the short bond length is 1.72(8) Å while it is 2.21(7) Å to the opposite apex. Thus, the cooperative displacement of the V═O bond in the $Sr_2V_3O_9$ chains is broken by the triclinic transformation, leading to a more disordered V^{4+} arrangement. This is the main reason for the observed differences in the magnetic susceptibilities of the Pb^{2+} and Sr^{2+} phases. An alternating $J_1 - J_2$ chain model was satisfactorily fitted for $Pb_2V_3O_9$ while a regular chain model matched the data for $Sr_2V_3O_9$.

Introduction

Interest in heavy metal phosphates, arsenates, and vanadates is driven by the promise of improved anion transport materials stimulated by the initial discovery of high ionic conductivity in $Bi_4V_2O_{11}$ and in the substituted BIMEVOX series of compounds.[1−3] Further, the effect of the $6s^2$ lone-pair electrons on the coordination polyhedra of highly polarizable Bi^{3+} and isoelectronic Pb^{2+} cations in these structures is of great chemical interest.[4−9] A recent investigation of the effect on crystal chemical and magnetic properties of the solid

* To whom correspondence should be addressed.

(1) Abraham, F.; Debreuille-Gresse, M. F.; Mairesse, G.; Nowogrocki, G. *Solid State Ionics* **1988**, *28−30*, 529.
(2) Abraham, F.; Boivin, J. C.; Mairesse, G.; Nowogrocki, G. *Solid State Ionics* **1990,** *40−41*, 934.
(3) Joubert, O.; Jouanneaux, A.; Ganne, M. *Mater. Res. Bull.* **1994**, *29*, 175.
(4) Moore, P. B.; Sen Gupta, P. K.; Le Page, Y. *Am. Miner.* **1989**, *74*, 1186.
(5) Galy, J.; Enjalbert, R. *J. Solid State Chem.* **1982**, *44*, 1.
(6) Mentre, O.; Abraham, F. *J. Solid State Chem.* **1996**, *125*, 91.
(7) Le Bellac, D.; Kiat, J. M.; Garnier, P. *J. Solid State Chem.* **1995**, *114*, 459.
(8) Morin, E.; Wallez, G.; Jaulmes, S.; Couturier, J. C.; Quarton, M. *J. Solid State Chem.* **1998**, *137*, 283.

10.1021/cm990073l CCC: $18.00
Published on Web 08/07/1999

solution series $Sr_{2-x}Pb_xV_3O_9$ has shown that as x increases the crystallographic sites occupied by Sr/Pb as well as the V sites progressively split. Eventually the crystal system changes from monoclinic to triclinic beyond $x \approx 1.5$.[10] For $x = 2$, crystals were grown but the structure was not determined. However, $Pb_2V_3O_9$ exhibited a more complex IR spectrum and the magnetic susceptibility indicated differences in the coupling between the V^{4+} ions when compared to its well-characterized strontium homologues. Because of these interesting changes we report here the crystal structure of this phase. We also present a more detailed study of the magnetic susceptibility for the solid solution series $Sr_{2-x}Pb_xV_3O_9$.

Experimental Section

$Pb_2V_3O_9$ crystals were prepared by the electrochemical reduction of PbV_2O_6 at 650 °C in an alumina crucible that was placed inside a sealed steel cylinder. A N_2 gas flow was maintained in the cylinder to prevent the melt from oxidizing. The electrolysis was carried out for 6 h using Ni electrodes. The applied potential was fixed at 3 V. During the 6 h experiment, the initial current of 200 mA gradually increased to 500 mA. This change is due to the appearance of a new phase and by a reaction occurring at the anode that formed black, parallelepiped crystals that were later shown by X-ray diffraction to be $Pb_2V_3O_9$.

Weissenberg diagrams and the resultant information obtained from the twinned crystals has been previously described.[10] It was hoped that a new preparation with somewhat different electrochemical parameters would produce single crystals. Unfortunately all crystals that we examined were twinned the same way as previously described. It is evident from the lattice parameters that $Pb_2V_3O_9$ is quasi-isostructural with $Sr_2V_3O_9$. However, the introduction of Pb^{2+} in place of Sr^{2+} gives rise to a significant distortion of the structure due to the $6s^2$ lone-pair stereochemical effect. Single-phase $Sr_{2-x}Pb_xV_3O_9$ specimens were prepared as previously described.[10] Knowing the twinning mechanism, a refinement of the structure was undertaken with a local program that requires an intensity data file that contains the contribution from each individual. To obtain the data, a large collimator and scan range were used for the intensity collection. However, this proved to be unsuccessful. It was therefore decided to employ Rietveld refinement of neutron and X-ray powder diffraction data instead.

To determine the slight triclinic distortion that $Pb_2V_3O_9$ has undergone by Rietveld refinement appears at first as an uncertain procedure. However, the distortion in the coordination polyhedron around Pb^{2+} due to the lone pair had been verified in the phase $Sr_{0.67}Pb_{1.33}V_3O_9$ that is still monoclinic.[10] Furthermore, X-ray and neutron diffraction play a complementary role in this determination. Neutron diffraction can clearly distinguish between Pb and oxygen while vanadium is not detectable. On the other hand, with X-ray diffraction data, it is very difficult to locate the oxygen ions in the presence of the heavy Pb atoms. A satisfactory crystal structure determination was achieved by the use of both sets of diffraction data. The FULLPROF 97 program[11] was used for the refinement. It does not allow a simultaneous X-ray/neutron refinement.

To facilitate the comparison of the refinement with that of $Sr_2V_3O_9$, $C2/c$, $a = 7.555(1)$ Å, $b = 16.275(2)$ Å, $c = 6.948(1)$ Å, $\beta = 119.78(1)°$, the unconventional triclinic space group $C\bar{1}$ was chosen. The lattice constants obtained by least squares refinement from the powder X-ray diffraction data are $a = 7.5956(3)$ Å, $b = 16.3927(4)$ Å, $c = 6.9707(2)$ Å, $\alpha = 91.38(1)°$, $\beta = 119.34(1)°$, $\gamma = 90.48(1)°$.

Table 1. Neutron and X-ray Data Collection and Rietveld Refinement for $Pb_2V_3O_9$

data collection	neutron	X-ray
diffractometer	ILL D2B	Siemens D5000
wavelengths	monochromator Ge (335)	Cu(Kα1 − Kα2)
1.5938 Å	1.54056 and 1.54439 Å	
2θ range (deg)	10−150	7−120
step scan (2θ, deg)	0.05	0.025
time/step	10 h total time	47 s
formula weight	711.2	711.2
space group	$C\bar{1}$	$C\bar{1}$
Z	2	2
cell parameters		
a, Å	7.5935(1)	7.5956(3)
b, Å	16.3898(3)	16.3927(4)
c, Å	6.9696(1)	6.9707(2)
α, deg	91.41(1)	91.38(1)
β, deg	119.34(1)	119.34(1)
γ, deg	90.49(1)	90.48(1)
V, Å^3	755.69	756.14
no. of reflections	1448	2245
no. of refined parameters	113	96
profile function	pseudo-Voigt ($\eta = 0.25(2)$)	pseudo-Voigt ($\eta = 0.92(4)$)
half-width parameters	$U = 0.030(2)$ $V = -0.086(4)$ $W = 0.106(2)$	$U = -0.001(2)$ $V = 0.012(1)$ $W = 0.0018(3)$
asymmetry parameters	0.15(1) to 0.06(1)	0.003(6) to 0.014(1)
$R_{wp} = [\sum_i w_i(y_i - y_{ci})^2/\sum_i w_i y_i^2]^{1/2}$	0.149	0.182
$R_p = \sum_i\|y_i - y_{ci}\|/\sum_i y_i$	0.131	0.161
$R_F = \sum\|\|F_{obs}\| - \|F_{calc}\|\|/\sum\|F_{obs}\|$	0.057	0.072
$R_{Bragg} = \sum\|I_k - I_k^{calc}\|/\sum I_k$	0.087	0.093
$\chi^2 = [R_{wp}/R_{exp}]^2$	6.64	2.75

Magnetic susceptibilities were measured with a Quantum-Design DC SQUID magnetometer over the range 6−200 K for five samples. The measurements were taken by equilibrating the sample at 6 K in an applied field of 1 kOe. The sample temperature was then raised in steps to 200 K, and measurements were made at each step. Previous measurements on $Sr_2V_3O_9$ and $Pb_2V_3O_9$ indicated perfect reversibility between ZFC and FC data for these compounds.[10] Susceptibility plots vs T were fitted according to a 12 $^1/_2$ spins ring chain using the program SPIN version 2.3.[12]

Neutron Powder Diffraction

The experimental data were collected at the Institute Laue-Langevin (ILL) at Grenoble, France, using the D2B powder diffractometer with conditions shown in Table 1. One data set was collected at 290 K and a second at 2 K. A total of 1448 independent reflections were fitted from the pattern profile. Because $Pb_2V_3O_9$ is nearly isostructural with $Sr_2V_3O_9$ the initial model for the Rietveld refinement was based on the structure of the latter. The atomic positions were refined, and the first difference Fourier map showed peaks adjacent to Pb. However, these maxima completely disappeared after anisotropic displacement parameters for Pb and

(9) Jakubowicz, N.; Perez, O.; Grebille, D.; Leligny, H. *J. Solid State Chem.* **1998**, *139*, 194.

(10) Mentre, O.; Dhaussy, A. C.; Abraham, F.; Steinfink, H. *J. Solid State Chem.* **1998**, *140*, 417.

(11) Rodriguez-Carjaval, J. FULLPROF 97; Laboratoire Leon Brillouin (CEA-CNRS): France.

(12) Maingot, F. SPIN version 2.3.7; IPCMS:, Stasbourg, France, 1997.

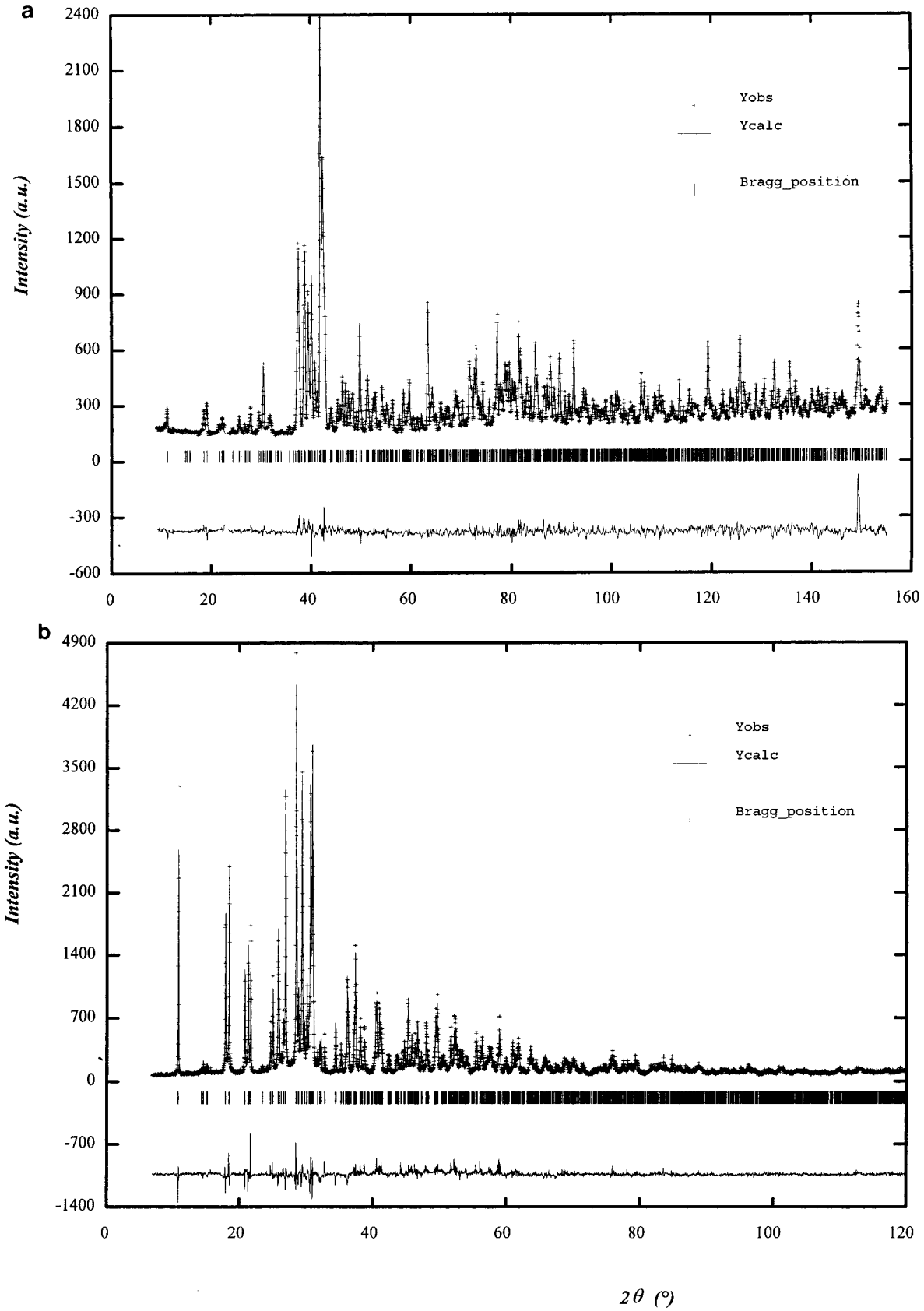

Figure 1. The calculated, observed, and difference diffraction profiles from (a) neutron and (b) X-ray data at 290 K for $Pb_2V_3O_9$.

O were introduced in the refinement cycles. At this point the vanadium atoms were not included. The final parameters were $\chi^2 = 6.64$, $R_{Bragg} = 8.67\%$, $R_f = 5.74\%$, $R_p = 13.1\%$, and $R_{wp} = 14.9\%$. The experimental and calculated diffraction patterns are shown in Figure 1a.

X-ray Powder Diffraction

Data were collected with a Siemens D5000 diffractometer over the range 2θ 7−120° in intervals of 0.025° and a count time of 47 s (Table 1). The examination of

Table 2. Atomic Coordinates, Occupancy and Isotropic Displacement Parameters Refined from (a) Neutron Data at 290 K, (b) X-ray Data at 290 K, and (c) Neutron Data at 2K[a]

atom	mult	occ		*x*	*y*	*z*	B_{eq} (Å^2)[b]
Pb(1)	4	1	a	−0.0063(8)	−0.1233(3)	0.2241(8)	2.09(4)
			b	−0.0053(7)	−0.1239(2)	0.2242(6)	1.60(3)
			c	0.0026(7)	−0.1213(3)	0.2172(9)	1.26(3)
Pb(2)	4	1	a	0.0111(9)	0.4513(3)	0.2469(7)	2.98(5)
			b	0.0095(6)	0.4511(2)	0.2461(6)	1.65(6)
			c	0.0165(7)	0.4530(3)	0.2487(7)	1.06(3)
$O(1)_a$	4	1	a	0.1478(10)	0.7334(4)	0.2058(11)	1.64(7)
			b	0.138(6)	0.732(2)	0.222(6)	1.64(0)
			c	0.1498(11)	0.7358(5)	0.2056(13)	1.14(13)
$O(1)_b$	4	1	a	0.8275(9)	0.7108(4)	0.2811(10)	1.67(16)
			b	0.856(6)	0.723(2)	0.271(6)	1.67(0)
			c	0.8134(11)	0.7071(5)	0.2786(13)	1.35(14)
$O(2)_a$	4	1	a	0.1635(9)	0.0251(5)	0.2239(11)	2.09(13)
			b	0.165(6)	0.047(2)	0.196(6)	2.09(0)
			c	0.1579(10)	0.0220(4)	0.2251(11)	0.58(11)
$O(2)_b$	4	1	a	0.8346(9)	0.0143(5)	0.2870(10)	2.91(12)
			b	0.863(7)	0.037(2)	0.283(6)	2.91(0)
			c	0.8358(11)	0.0158(5)	0.2912(13)	1.18(13)
$O(3)_a$	4	1	a	0.4193(10)	0.0880(4)	0.0461(11)	2.05(14)
			b	0.425(7)	0.098(2)	0.102(7)	2.05(0)
			c	0.4258(11)	0.0858(4)	0.0500(12)	0.85(11)
$O(3)_b$	4	1	a	0.6547(11)	0.1064(4)	0.4941(10)	1.88(13)
			b	0.644(6)	0.120(2)	0.471(7)	1.88(0)
			c	0.6554(12)	0.1116(5)	0.4978(13)	0.90(11)
$O(4)_a$	4	1	a	0.8409(12)	0.1358(4)	0.0211(12)	2.06(17)
			b	0.819(6)	0.137(2)	−0.001(7)	2.06(0)
			c	0.8398(11)	0.1340(4)	0.0228(12)	0.82(12)
$O(4)_b$	4	1	a	0.1302(10)	0.1448(4)	0.4978(10)	1.97(12)
			b	0.152(5)	0.141(2)	0.532(6)	1.97(0)
			c	0.1187(11)	0.1439(5)	0.5014(13)	1.02(13)
O(5)	4	1	a	0.0043(8)	0.2855(3)	0.2536(10)	1.29(12)
			b	0.008(7)	0.290(2)	0.242(7)	1.29(0)
			c	0.0096(11)	0.2880(5)	0.2565(12)	0.99(12)
V(1)	4	1	b	0.0084(31)	0.6614(8)	0.2649(23)	5.53(7)
V(2)	4	1	b	−0.0045(21)	0.0857(7)	0.2537(25)	2.29(8)
$V(3)_a$	4	0.5	b	0.2645(90)	0.7594(30)	−0.0220(82)	0.97(7)
$V(3)_b$	4	0.5	b	0.7102(59)	0.7521(25)	0.4726(69)	1.38(6)

[a] Vanadium parameters were only refined from X-ray data. [b] $B_{eq} = {}^4/_3 \sum i \sum j \beta_{ij} a_i a_j$.

Table 3. Anisotropic Displacement Parameters of Pb Atoms for $Pb_2V_3O_9$ (a) from Neutron Data at 290 K, (b) from X-ray Data at 290 K, and (c) from Neutron Data at 2K[a]

atom		β_{11}	β_{22}	β_{33}	β_{12}	β_{13}	β_{23}
Pb(1)	a	0.0119(9)	0.0020(2)	0.0167(12)	0.0014(3)	0.0087(9)	0.0013(4)
	b	0.0294(8)	0.0026(2)	0.0214(18)	0.0004(5)	0.0109(15)	−0.0002(5)
	c	0.0032(9)	0.0010(2)	0.0192(17)	0.0011(3)	0.0085(10)	0.0001(4)
Pb(2)	a	0.0342(18)	0.018(2)	0.0148(14)	0.0020(4)	0.0181(13)	0.0011(4)
	b	0.0276(20)	0.0036(3)	0.0202(18)	−0.0016(5)	0.0126(16)	−0.0009(5)
	c	0.0080(10)	0.0011(2)	0.0012(11)	−0.0015(3)	0.0004(9)	−0.0011(3)

[a] The anisotropic displacement exponent takes the form $-(\beta_{11}h^2 + \beta_{22}k^2 + \beta_{33}l^2 + 2\beta_{12}hk + 2\beta_{13+}hl + 2\beta_{23}kl)$.

several diffraction diagrams obtained from different samples showed that the patterns were subject to preferred orientation, in particular the 0*k*0 reflections showed pronounced enhancement of their intensities. To correct this the (010) preferred orientation March function[13,14] was introduced into the refinement process. Despite these corrections, not all of the preferred orientation effect could be removed, and it is the main reason for the relatively high values *R*. The initial atomic positions for Pb and O atoms were those from the refinement of the neutron diffraction data. Positional and isotropic displacement parameters for V were obtained from the Rietveld refinement. The V(1) and V(2) sites are fully occupied while the $V(3)_a$ and $V(3)_b$ sites have an occupancy of $^1/_2$ in agreement with the $Sr_2V_3O_9$ crystal structure. The introduction of oxygen with refined isotropic displacement parameters improved the refinement somewhat but the latter parameters had large esd's. The oxygen displacement parameters were therefore fixed using the values obtained from the neutron data. The final refinement carried out with anisotropic displacement parameters for Pb and V yielded $\chi^2 = 2.75$, $R_{Bragg} = 9.27\%$, $R_f = 7.23\%$, $R_p = 16.1\%$, and $R_{wp} = 18.2\%$. The experimental and calculated patterns are shown in Figure 1b. Tables 2 and 3 list the atomic coordinates and displacement parameters. Table 4 lists selected bond lengths and angles. The Pb−O distances are calculated from coordinates obtained from neutron data refinement while the V−O distances are based on X-ray data.

Lone-Pair Localization

The interplay among lone-pair electrons, stereochemistry, and crystal structure has long been of interest to crystallographers and solid-state chemists.[5,9,15] The

(13) March, A. *Z. Kristallogr.* **1932**, *81*, 285.
(14) Dollase, W. A. *J. Appl. Crystallogr.* **1986**, *19*, 267.
(15) Shimoni-Livny, Liat; Glusker, Jenny P.; Bock, Charles W. *Inorg. Chem.* **1998**, *37*, 1853.

Table 4. Selected Distances (Å) and Angles (deg) with Standard Deviations in Parentheses for $Pb_2V_3O_9$ Refined from Neutron and X-ray Data[a]

Pb(1) environment		Lp−O	Lp−Pb(1)−O
Pb(1)−O(1)$_a$	2.661(9)	2.624	80.1
Pb(1)−O(2)$_a$	2.744(9)	3.275	154.3
Pb(1)−O(2)$_b$	2.694(10)	2.817	96.1
Pb(1)−O(3)$_a$^{ii}	2.830(8)	2.551	56.1
Pb(1)−O(3)$_b$^{ii}	2.426(8)	2.863	134.5
Pb(1)−O(4)$_a$^{ii}	2.575(12)	2.920	121.5
Pb(1)−O(4)$_b$^{ii}	2.566(11)	2.274	54.3
Pb(2) environment		**Lp−O**	**Lp−Pb(2)−O**
Pb(2)−O(2)$_a$^{iii}	2.847(10)	2.515	49.9
Pb(2)−O(2)$_b$^{iii}	2.540(10)	3.057	151.4
Pb(2)−O(3)$_a$^{iii}	2.588(8)	2.874	115.7
Pb(2)−O(3)$_a$^{iv}	2.421(11)	2.887	139.7
Pb(2)−O(3)$_b$^{iii}	2.918(8)	3.053	97.1
Pb(2)−O(3)$_b$^{iv}	2.833(11)	2.271	12.3
Pb(2)−O(4)$_a$^{iv}	2.753(8)	2.539	61.7
Pb(2)−O(4)$_b$^{iv}	2.920(8)	3.074	101.0
Pb(2)−O(5)	2.719(7)	2.594	71.4

V(1) environment		V(2) environment	
V(1)−O(1)$_a$	1.76(2)	V(2)−O(2)$_a$	1.71(2)
V(1)−O(1)$_b$	1.65(2)	V(2)−O(2)$_b$	1.78(2)
V(1)−O(3)$_a$^{iii}	1.76(2)	V(2)−O(4)$_a$	1.70(1)
V(1)−O(3)$_b$^{iii}	1.72(2)	V(2)−O(4)$_b$	1.75(2)
O(1)$_a$−V(1)−O(1)$_b$	107.3(1)	O(2)$_a$−V(2)−O(2)$_b$	103.5(1)
O(1)$_a$−V(1)−O(3)$_a$^{iii}	105.0(1)	O(2)$_a$−V(2)−O(4)$_a$	113.0(1)
O(1)$_a$−V(1)−O(3)$_b$^{iii}	113.5(1)	O(2)$_a$−V(2)−O(4)$_b$	108.0(1)
O(1)$_b$−V(1)−O(3)$_a$^{iii}	114.0(1)	O(2)$_b$−V(2)−O(4)$_a$	105.2(1)
O(1)$_b$−V(1)−O(3)$_b$^{iii}	113.0(1)	O(2)$_b$−V(2)−O(4)$_b$	109.1(1)
O(3)$_a$^{iii}−V(1)- O(3)$_b$^{iii}	103.9(1)	O(4)$_a$−V(2)−O(4)$_b$	117.2(1)

V(3)$_a$ environment		V(3)$_b$ environment	
V(3)$_a$−O(1)$_a$	2.21(7)	V(3)$_b$−O(1)$_b$	2.04(6)
V(3)$_a$−O(1)$_a$^{iv}	1.72(8)	V(3)$_b$−O(1)$_b$^{iv}	1.96(5)
V(3)$_a$−O(4)$_a$^{ii}	1.90(6)	V(3)$_b$−O(4)$_b$^{ii}	2.02(4)
V(3)$_a$−O(4)$_a$^{iii}	2.10(5)	V(3)$_b$−O(4)$_b$^{iii}	1.90(4)
V(3)$_a$−O(5)^{ii}	2.00(5)	V(3)$_b$−O(5)^{ii}	2.18(4)
V(3)$_a$−O(5)^{iii}	1.92(4)	V(3)$_b$−O(5)^{iii}	1.67(4)
O(1)$_a$−V(3)$_a$−O(1)$_a$^{iv}	172.8(1)	O(1)$_b$−V(3)$_b$−O(1)$_b$^{iv}	164.7(1)
O(1)$_a$−V(3)$_a$−O(4)$_a$^{ii}	82.4(1)	O(1)$_b$−V(3)$_b$−O(4)$_b$^{ii}	84.2(1)
O(1)$_a$−V(3)$_a$−O(4)$_a$^{iii}	82.9(1)	O(1)$_b$−V(3)$_b$−O(4)$_b$^{iii}	91.5(1)
O(1)$_a$−V(3)$_a$−O(5)^{ii}	84.2(2)	O(1)$_b$−V(3)$_b$−O(5)^{ii}	84.7(1)
O(1)$_a$−V(3)$_a$−O(5)^{iii}	80.8(2)	O(1)$_b$−V(3)$_b$−O(5)^{iii}	91.7(1)
O(1)$_a$^{iv}−V(3)$_a$−O(4)$_a$^{ii}	104.2(2)	O(1)$_b$^{iv}−V(3)$_b$−O(4)$_b$^{ii}	90.5(1)
O(1)$_a$^{iv}−V(3)$_a$−O(4)$_a$^{iii}	90.4(2)	O(1)$_b$^{iv}−V(3)$_b$−O(4)$_b$^{iii}	89.8(1)
O(1)$_a$^{iv}−V(3)$_a$−O(5)^{ii}	92.4(2)	O(1)$_b$^{iv}−V(3)$_b$−O(5)^{ii}	80.4(1)
O(1)$_a$^{iv}−V(3)$_a$−O(5)^{iii}	101.8(2)	O(1)$_b$^{iv}−V(3)$_b$−O(5)^{iii}	102.9(1)
O(4)$_a$^{ii}−V(3)$_a$−O(4)$_a$^{iii}	165.1(2)	O(4)$_b$^{ii}−V(3)$_b$−O(4)$_b$^{iii}	164.5(1)
O(4)$_a$^{ii}−V(3)$_a$−O(5)^{ii}	92.6(2)	O(4)$_b$^{ii}−V(3)$_b$−O(5)^{ii}	83.1(1)
O(4)$_a$^{ii}−V(3)$_a$−O(5)^{iii}	91.1(2)	O(4)$_b$^{ii}−V(3)$_b$−O(5)^{iii}	92.4(1)
O(4)$_a$^{iii}−V(3)$_a$−O(5)^{ii}	83.5(2)	O(4)$_b$^{iii}−V(3)$_b$−O(5)^{ii}	91.7(1)
O(4)$_a$^{iii}−V(3)$_a$−O(5)^{iii}	89.0(2)	O(4)$_b$^{iii}−V(3)$_b$−O(5)^{iii}	102.6(1)
O(5)^{ii}−V(3)$_a$−O(5)^{iii}	163.9(2)	O(5)^{ii}−V(3)$_b$−O(5)^{iii}	174.5(1)

O−O characteristic bonds			
O(4)$_a$−O(4)$_b$	2.950(9)	O(5)−O(5)^{iv}	3.887(9)
O(5)−O(5)^{iv}	3.845(10)		

[a] Symmetry operations: ii, $^1/_2 + x$, $^1/_2 + y$, z; iii, $-x$, $-y$, $-z$; iv, $^1/_2 - x$, $^1/_2 - y$, $-z$.

theory enabling the calculation for localizing the lone-pair electrons in a crystal structure was developed by Verbaere et al.[16] It is based on the local electric field calculation in the whole crystal using Ewald's method[17] and was recently successfully applied to several materials.[7−9] It was incorporated in the computer program HYBRIDE. The polarizability for Pb^{2+} was chosen as α = 6.583 Å^3.[18] After an ionic model and a partial charge model for the atom was considered, satisfactory, self-consistent, lone-pair electron positions were obtained by the latter. The mean ionicity for each M chemical species was calculated for $Pb_2V_3O_9$ from the electronegativity differences of the terminal atoms of the M−O bonds. Thus, a % formal ionicity value was calculated for each bond using the formula

$$\mathrm{M{-}O} = 1 - \exp[-(X_\mathrm{O} - X_\mathrm{M})^2/4]$$

It was then applied to the oxidation state of the cation. This procedure yields +1.22 for Pb^{2+}, +2.60 for V^{4+}, and +3.25 for V^{5+}. The different oxygen atoms were given the balancing −1.21 charge to ensure electroneutrality within the lattice. The program HYBRIDE splits the polarizable Pb^{2+} into a mobile −2 charge for the lone-pair electrons and a stationary +3 charge for the nu-

Table 5. Lone Pair (Lp) Position[a]

atom	Lp fractional coordinates	core−Lp distance (Å)	
Pb(1)	$x = -0.072$	$d = 0.58$	$d_x = -0.63$
	$y = -0.145$		$d_y = -0.18$
	$z = 0.212$		$d_z = -0.08$
Pb(2)	$x = 0.961$	$d = 0.57$	$d_x = -0.42$
	$y = 0.441$		$d_y = 0.09$
	$z = 0.283$		$d_z = 0.22$

[a] d_x, d_y, and d_z are the nucleus−Lp distances projected along x, y, and z.

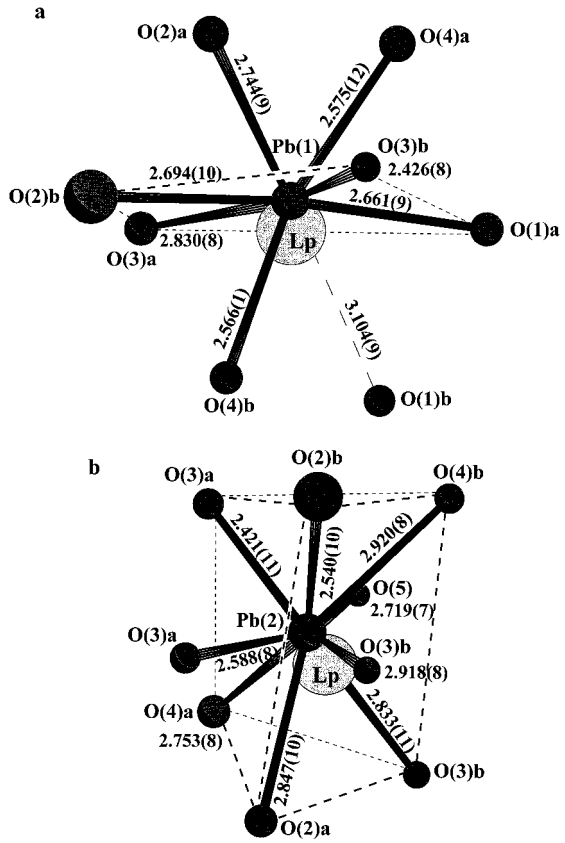

Figure 2. Lead cations and lone-pair environment: (a) distorted, capped octahedron for the Pb(1) atom and (b) tricapped trigonal prism for the Pb(2) atom.

(16) Verbaere, A.; Marchand, R.; Tournoux, M. *J. Solid State Chem.* **1978**, *23*, 383.

(17) Ewald, P. P. *Ann. Phys.* **1921**, *64*, 253.

(18) Shannon, R. D. *Acta Crystallogr.* **1976**, *A32*, 751.

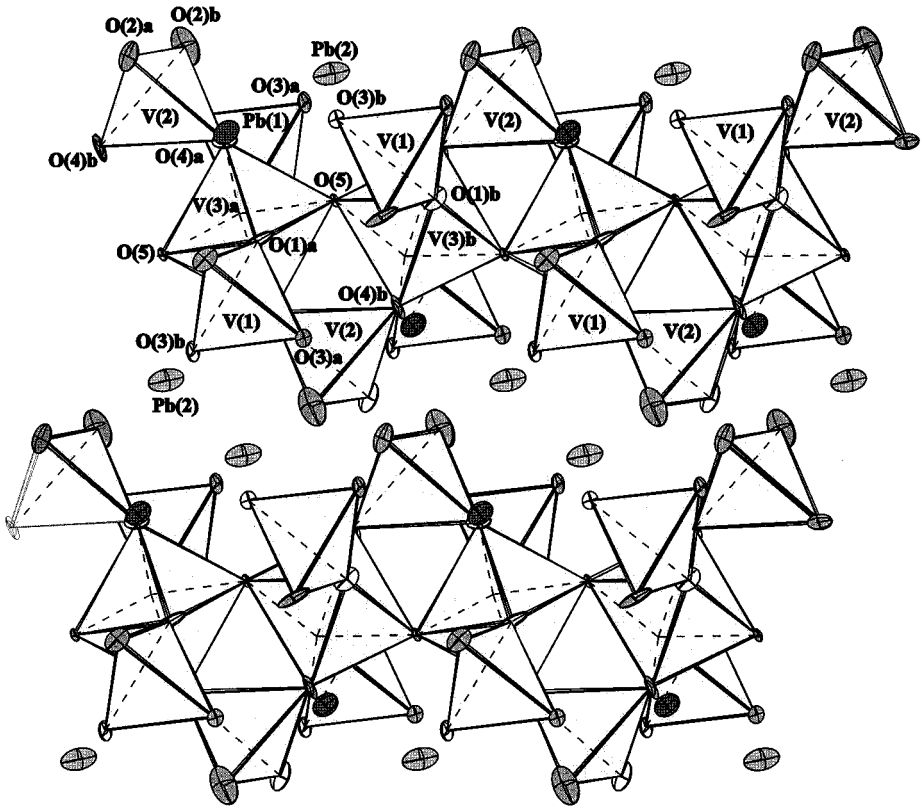

Figure 3. Two layers of $Pb_2V_3O_9$ projected on (101).

cleus and the core orbitals. The refinement of the lone-pair positions for both Pb(1) and Pb(2) placed them 0.58 and 0.57 Å, respectively, from the nucleus (Table 5).

Description of the Structure

The structure of $Pb_2V_3O_9$ is nearly isostructural with $Sr_2V_3O_9$. The replacement of Sr by Pb, which contains a nonbonding $6s^2$ electron pair, gives rise to a triclinic distortion. Thus, the coordination polyhedra of the lead ions are distorted compared to the more regular coordination around Sr. Pb(1) is coordinated to seven oxygen ions that form a distorted capped octahedron (Figure 2a), and it is essentially the same as found in Pb_4BiPO_8.[19] The Pb−O bonds in Pb_4BiPO_8 range from 2.14(2) Å to 3.16(3) Å. In $Pb_2V_3O_9$, they range from 2.426(8) Å to 2.830(8) Å. The four atoms $O(1)_a$, $O(3)_a$, $O(2)_b$, and $O(3)_b$ lie nearly in a plane with Pb(1) slightly above it. They form a distorted equatorial plane of an octahedron whose vertexes are occupied by $O(4)_a$ and $O(4)_b$; $O(2)_a$ caps the triangular face $O(2)_b-O(3)_b-O(4)_a$. At a somewhat longer distance [3.104(9) Å] $O(1)_b$ caps the opposite triangular face $O(1)_a-O(3)_a-O(4)_b$. The distortions open a space opposite $O(1)_b$ where the $6s^2$ electrons are nested. The valence bond sum is 1.76.[20] The contribution of the long $Pb(1)-O(1)_b$ is negligible.

Pb(2) is surrounded by nine oxygen ions that form a distorted tricapped, trigonal prism (Figure 2b). This configuration is sometimes observed for heavy metal cations, e.g., Bi^{3+} in $Bi_3Ru_3O_{11}$.[21] The range of Pb(2)−O bond lengths is 2.421(11) Å to 2.920(8) Å. The valence bond sum is 1.9. The $Pb(2)-O(4)_b$, $Pb(2)-O(3)_b^{iii}$, $Pb(2)-O(3)_b^{iv}$, and $Pb(2)-O(2)_a$ are considerably longer than the other five bonds due to Coulomb repulsion from the $6s^2$ electrons.

Of the four crystallographically independent vanadium atoms, V(1) and V(2) are in tetrahedral coordination with a mean oxidation number +5. $V(3)_a$ and $V(3)_b$ are in octahedral coordination with oxidation number +4. The octahedra link by corner sharing into an infinite chain parallel to the [101] direction. The tetrahedra share corners with the octahedra to form two-dimensional sheets that are then joined by the Pb ions into a three-dimensional structure, Figure 3. The $V(3)_b$ cations show similar displacements from their polyhedral centers as seen in $Sr_2V_3O_9$[10] and $Ba_2V_3O_9$[22], giving rise to a short vanadyl bond, $V(3)_b-O(5) = 1.67(4)$ Å and a long $V(3)_b-O(5)$ bond of 2.18(4) Å (Figure 4a). The main difference between the lead and strontium vanadate framework is in the displacement of $V(3)_a$ toward $O(1)_a$, which is corner-shared with a V(1) tetrahedron. The $V(3)_a-O(1)_a$ short bond length is 1.72(8) Å while it is 2.21(7) Å to the opposite apex $O(1)_a$ ion. Thus, the cooperative displacement of the V═O bond in the $Sr_2V_3O_9$ chains is broken by the triclinic transformation, leading to a more disordered V^{4+} arrangement (Figure 4a,b). This is the main reason for the observed differences in the magnetic susceptibilities as Pb^{2+} substitutes for Sr^{2+}.

The Pb(2) ions connecting two octahedral layers parallel to [010] display a large anisotropic displacement

(19) Giraud, S.; Wignacourt, J. P.; Drache, M.; Nowogrocki, G.; Steinfink, H. *J. Solid State Chem*. **1999**, *142*, 80.
(20) Brown, I. D.; Altermatt, D. *Acta Crystallogr*. **1985**, *B41*, 244.
(21) Abraham, F.; Trehoux, J.; Nowogrocki, G. *Bull. Soc. Fr. Mineral. Cristallogr*. **1975**, *98*, 25.
(22) Dhaussy, A. C.; Mentre, O.; Abraham. F.; Steinfink, H. *J. Solid State Chem*. **1996**, *126*, 328.

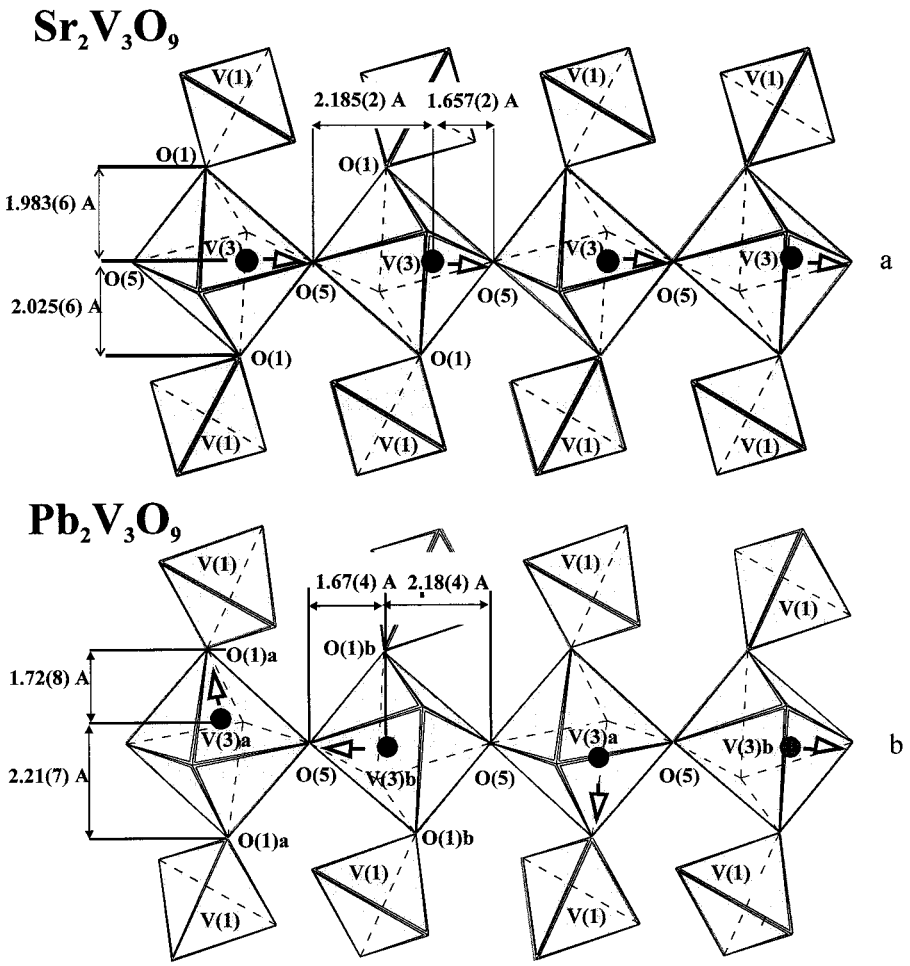

Figure 4. Vanadium displacements to form vanadyl bonds within the octahedral chains for (a) $Sr_2V_3O_9$ and (b) $Pb_2V_3O_9$.

parameter parallel to [101]. Similarly large anisotropic displacement values are seen for the oxygen ions of the V(2) tetrahedron, and the V(1) and V(2) displacement parameters are also large. This observation is reminiscent of the local disorder seen in $Sr_{0.67}Pb_{1.33}V_3O_9$.[10] The reduction of the symmetry from monoclinic to triclinic cannot completely take care of the local disorder. In fact the large vibration ellipses affect the bond lengths because the actual position of the atoms is dynamically disordered over two close, adjacent sites.

Low-Temperature Data

To test the hypothesis that the displacements are not purely of thermal origin a neutron diffraction data set was collected at 2 K and refined. The lattice parameters are $a = 7.5839(2)$ Å, $b = 16.3349(3)$ Å, $c = 6.9547(2)$ Å, $\alpha = 91.64(1)°$, $\beta = 119.24(1)°$, and $\gamma = 90.80(1)°$; the positional parameters and bond lengths remain the same within 3σ (Table 2). The displacement parameters for the Pb and O ions decreased as expected. However, the shape of the anisotropic triaxial ellipsoids for the Pb(1) and Pb(2) remains the same as for the high-temperature data (Table 3). Final reliability factors were $R_{Bragg} = 10.2\%$, $R_f = 5.57\%$, $R_p = 13.7\%$, and $R_{wp} = 20.4\%$.

The magnetic structure refinement is uncertain since the detected antiferromagnetic order within the chains conserves the nuclear unit cell, i.e., 2 V^{4+} of the same chain per unit cell. Thus, Bragg magnetic intensities are superposed on nuclear peaks and are expected to be weak because of the d^1 magnetic ions. The transparent nuclear character of vanadium toward neutrons enhances these difficulties. However, two V^{4+} ions were refined. V(3) at $x = 0.285(10)$, $y = 0.755(4)$, $z = 0.023(1)$ and V(4) at $x = 0.727(11)$, $y = 0.757(4)$, $z = 0.480(11)$, forming short V(3)−V(4) distances of 3.32(10) Å. The 1 μB magnetic moment was subsequently fixed ferromagnetically and then antiferromagnetically parallel to the chain axisk, yielding, respectively, R_{magn} =53.5% and 5.2%. A slight tilt of all the spins of 15° yielded $R_{magn} = 2.5\%$.

Magnetic Susceptibility

Figure 5a−e show the variation of the susceptibility as a function of the Pb content and summarize the effective magnetic moments and the negative Curie−Weiss constants, θ, for these phases. The magnetic interaction decreases with increasing Pb content. For all of the phases the χT product vs T gradually increases in the paramagnetic region, confirming antiferromagnetic coupling. At the lowest temperature the slope is enhanced for the lead-rich part of the solid solution. $Sr_2V_3O_9$ is antiferromagnetic with a broad maximum at about 50 K (Figure 5a),[10] and its effective moment is 1.96 μ_B. It is larger than the theoretical value of 1.73 μ_B for spin only V^{4+} and is comparable with the value observed in $Ba_2V_3O_9$, 2 μ_B.[22] Data to at least 300 K may be necessary for an accurate Curie−Weiss fit. The

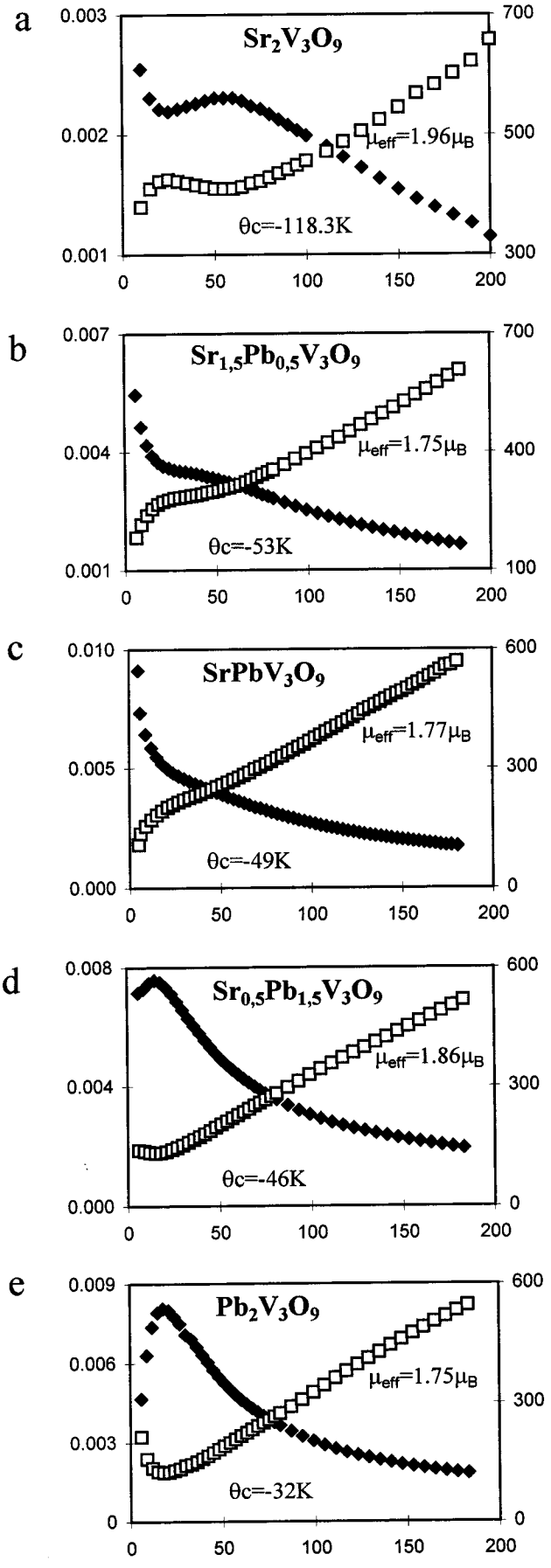

Figure 5. Temperature dependence of magnetic susceptibility (filled squares) and inverse susceptibility (open squares) for $Sr_{2-x}Pb_xV_3O_9$ solid solution phases.

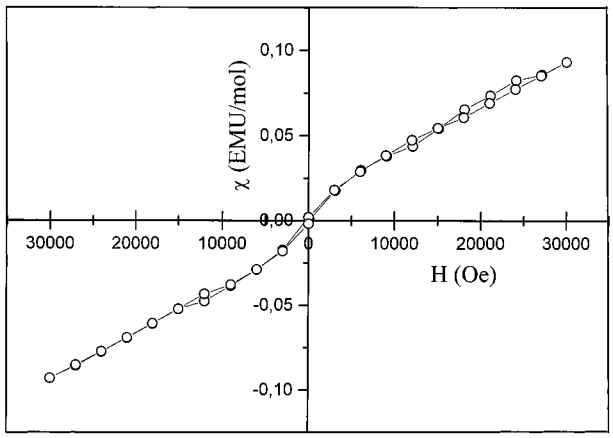

Figure 6. χ vs H hystereris cycle at 5 K for $Sr_2V_3O_9$.

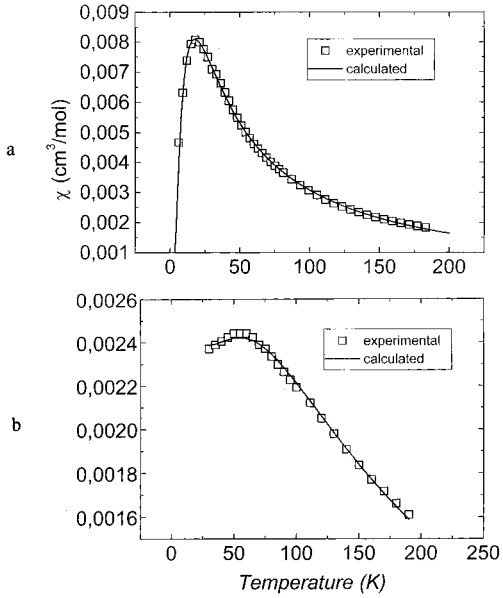

Figure 7. Experimental and calculated χ vs T plots for (a) $Pb_2V_3O_9$, $J_1 - J_2$ chain; (b) $Sr_2V_3O_9$, $J_1 - J_1$ chain + weak paramagnetism.

sudden increase in the susceptibility of $Sr_2V_3O_9$ at about 20 K was initially thought to be due to a canted spin structure. However, the χ vs H curve shows no hysteresis and essentially is characteristic of antiferromagnetic behavior (Figure 6). Thus, the progressive, systematic changes in the low-temperature susceptibility response as the composition changes from $Sr_2V_3O_9$ to $Pb_2V_3O_9$ are an intrinsic property of the materials. We assign it to the paramagnetic participation of noncoupled end-of-chain V^{4+}. To distinguish between several models (a) formation of dimers (Bleaney Bowers[23]), (b) alternating spins within chains, and (c) parallel spins within chains, the χ vs T $Sr_2V_3O_9$ curve was fit with an alternating $J_1 - J_2$ exchange from 30 to 290 K. The spin interaction was described by a Heisenberg model, $S_x \approx S_y \approx S_z$, likely for the vanadyl ion. Even though the experimental and calculated data did not match perfectly it led to strictly equal values of J_1 and J_2. Thereafter the refinement converged satisfactorily with the addition of a C/T paramagnetic term in a $J_1 - J_1$ regular chain model. The paramagnetic/antiferromagnetic sus-

(23) Bleaney, B.; Bowers, K. D. *Proc. R. Soc. London* **1952**, *A214*, 451.

Table 6. Results of the χ vs T Susceptibility Fit[a]

	J_1 (K)	J_2 (K)	g (Landé factor)	fit agreement (%)
$Pb_2V_3O_9$	−29.2	−19.3	1.93	0.44
$Sr_2V_3O_9$	−106.8	= J1	2.09	0.09

[a] The fit agreement value is given by $\Sigma_i(\chi_{calc} - \chi_{exp})^2/\Sigma(\chi_{exp}^2)$. $Sr_2V_3O_9$ was fitted with 3.9% of paramagnetic contribution.

ceptibility ratio was refined to 3.9%. Results of the fits are shown in Figure 7 and Table 6 and confirm the cooperative displacement of V^{4+} toward the bridging O(9) oxygen within the $Sr_2V_3O_9$ octahedral chains.

For the richest Pb phases, $Sr_{1.5}Pb_{0.5}V_3O_9$ and $SrPbV_3O_9$, the paramagnetic participation is still important but the lower Curie−Weiss temperature suggests a progressive weakening of the magnetic coupling with increasing presence of Pb^{2+} near the V^{4+} cations. Nevertheless, the sharp rises in the susceptibility at the low temperatures up to $x = 1$ suggests a tendency for V^{4+} to form dimers along the chains. This effect is further accentuated for $Pb_2V_3O_9$. In the triclinic domain V^{4+} is present in two, half-occupied, independent crystallographic sites labeled V(3) and V(4). A possible ordering would consist in the alternation of short, 3.45 Å, and long, 3.94 Å, V−V interactions. A model with alternate $J_1 - J_2$ chains without any paramagnetic contribution satisfactorily converged to a J_1/J_2 ratio of about $^2/_3$, Figure 7 and Table 6. It should be noted that $|J_1|$ $Sr_2V_3O_9 \gg |J_1|, |J_2|$ $Pb_2V_3O_9$ in good agreement with the Curie−Weiss temperature data. One can postulate that the end-of-chain vanadium atoms are coupled via J_1 to their neighbors and thus avoid a paramagnetic contribution to the susceptibility. This phenomenon is expected to gradually vanish until the triclinic/monoclinic composition limit is reached. A complete study of the magnetic properties for these materials is currently in progress.

Acknowledgment. O.M. and H.S. gratefully acknowledge the support for this research by the R. A. Welch Foundation, Houston, Texas. We are grateful to Dr. Gilles Wallez, Laboratoire de Cristallochimie du Solide, CNRS URA 1388, University Paris IV, France, for providing the HYBRIDE program and helpful advice in its use. The authors also acknowledge Professor G. Nowogrocki, LCPS, CNRS URA 452, Villeneuve d'Ascq for help with computer programming. Finally, we acknowledge the help of Dr. Marc Drillon and Dr. Pierre Rabu, IPCMS, CNRS UMR 7504, Strasbourg, France, for their detailed discussions and help with the magnetic fits.

CM990073L